Eur. Phys. J. B **14**, 227–238 (2000)

THE EUROPEAN PHYSICAL JOURNAL B

EDP Sciences

Order-disorder evolution in solid solutions of the NLO material $KTiOPO_4$: $K_{0.88}Rb_{0.12}TiOPO_4$ and $K_{0.465}Rb_{0.535}TiOPO_4$ in the temperature range 293-973 K*

P. Delarue[1], C. Lecomte[1,a], M. Jannin[2], G. Marnier[2], and B. Menaert[2]

[1] Laboratoire de Cristallographie et Modélisation des Matériaux Minéraux et Biologiques[b], Université Henri Poincaré, Nancy I, Faculté des sciences, BP 239, 54506 Vandœuvre-lès-Nancy Cedex, France
[2] Laboratoire de Physique de l'Université de Bourgogne[c], Faculté des sciences Mirande, BP 400, 21011 Dijon Cedex, France

Received 22 April 1999

Abstract. $K_{0.88}Rb_{0.12}TiOPO_4$ and $K_{0.465}Rb_{0.535}TiOPO_4$ solid solutions of the potassium titanyl phosphate ($KTiOPO_4$, space group $Pna2_1$) family, are described at 293, 473, 673, 873 and at 973 K. Their high resolution structures are obtained by using accurate single-crystal X-ray diffraction techniques at high resolution, $(\sin\theta/\lambda)_{max} = 1.36$ Å^{-1}. Large anharmonic motion of alkaline ions increasing with temperature allows the evolution of the rubidium and potassium ions repartition in the two alkaline sites *versus* temperature. To describe this motion inducing ionic conductivity phenomenon and to determine accurately the order-disorder evolution, two alkaline site refinement models are developed and discussed. A thermodynamic model, which uses a barrier-potential model, is also developed to specify the different interactions operating in the order-disorder evolution, and more generally interactions between alkaline ions and the framework.

PACS. 66.30.Hs Self-diffusion and ionic conduction in nonmetals – 42.70.Mp Nonlinear optical crystals – 64.60.Cn Order-disorder transformations; statistical mechanics of model systems

1 Introduction

Potassium titanium oxide phosphate, $KTiOPO_4$ (KTP) is a well-known nonlinear optical material which is extensively used for frequency conversion. Its chemical and thermal stability, as with its other properties, make it very interesting for technical applications. At room temperature and pressure, KTP crystallises in the acentric $Pna2_1$ space group [1]. Two crystallographically different distorted TiO_6 octahedra are linked through corners, alternately cis and trans, to form unidimensional chains, which are oriented along the c optic axis [0 0 1] [2] (Fig. 1). These alternating long- and short-bond Ti-O chains are bridged by PO_4 tetrahedra forming an open framework containing channels parallel to the c axis. The two potassium cations K^+, not symmetry related in the $Pna2_1$ phase, lying in those channels, are relatively free to migrate and contribute to the high anisotropic ionic conductivity of the KTP material. At high temperature, the KTP structure shows a reversible ferroelectric to paraelectric phase transition [3]. The Curie temperature (T_c) of KTP is close to 1218 K [3,4], depending on the crystal growth conditions, and its high temperature phase space group is Pnan [5]. In this phase, the titanium octahedra are centrosymmetric and the two potassium cations K^+ are symmetry related *via* the inversion center.

The KTP structure is very versatile with respect to isomorphous substitution. The potassium cation has been replaced totally or partially by Na^+, Rb^+, Tl^+, Cs^+, Ag^+, Li^+ and NH_4^+, whereas the titanium centre may be substituted by Ge^{4+}, Sn^{4+}, Zr^{4+} cations and heterovalent cations as Sb^{5+} or Ta^{5+} (which may induce lacuna on the other sites); in that latter case the electric balance may also induce the substitution of phosphorus by germanium. Finally arsenic atoms may replace the phosphorus (leading to MTA arseniate type materials) [6–23]. Solid solutions exist between many of these species, allowing selective modification of the non-linear optical properties [6–9]. These various compounds were studied in different ways to try to understand the correlations between the optical non-linearities (measured as second harmonic generation (SHG)) and the structural distortions. If the distorted octahedron, due to the short and long Ti-O bonds, seems to be directly correlated with the SHG properties [10–12], however the alkaline sites should not be neglected [8,9].

All these above properties make this material very suitable for manufacturing optical waveguides in

* Annexes are only available electronically at http://www.edpsciences.org

[a] e-mail: lecomte@lcm3b.u-nancy.fr
[b] LCM^{3}B ESA CNRS 7036
[c] LPUB UPRESA 5027

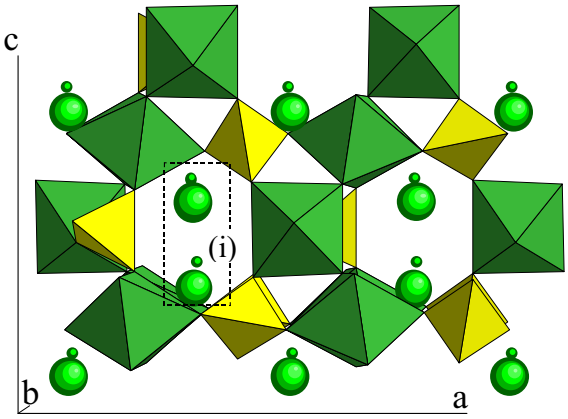

Fig. 1. View of $KTiOPO_4$ structure, at 293 K, along the b axis. The split positions of each potassium (sp) obtained at 973 K and the part of the structure (i) which enclosed the two potassium sites (K(1) and K(2)) are represented.

the crystal: waveguides have been obtained by ion exchange in which univalent ions such as rubidium, thallium or caesium replace the KTP potassium ions [13], or, more recently, caesium replaces the rubidium of $RbTiOAsO_4$ [14]. These waveguides may also be obtained by liquid phase epitaxy [15]. Precise knowledge of the physical properties of the alkaline ions in the KTP family would allow a better control of these processes. Moreover, at room temperature, the presence of two crystallographically distinct K, Ti and P sites introduces the possibility of substituent ordering. Complete or partial cation ordering has been observed [16–20]. But this order-disorder phenomenon and its evolution is not yet well understood.

The present work first reports on the variation of $K_{0.88}Rb_{0.12}TiOPO_4$ (KRb12TP) and $K_{0.465}Rb_{0.535}TiOPO_4$ (KRb535TP) lattice parameters, every 50 K from room temperature to 973 K; we then describe the accurate crystal structures modifications from single crystal X-ray diffraction data collected at 293, 473, 673, 873, 973 and 293 K. The evolution of the structure and of its properties *versus* temperature is very similar to what we have observed in $RbTiOPO_4$ (RbTP) and KTP [11,24]: we describe precisely the motion of the alkaline sites by using, besides an anharmonic refinement, a model, which splits the cation sites. This model is discussed considering the results obtained on germanate analogues of the KTP structure [21–23]. The order-disorder alkaline evolution is also studied *versus* temperature up to 973 K. Finally a thermodynamic model is proposed describing the order-disorder evolution.

2 Data collection

KRb12TP and KRb535TP crystals were grown by the flux-growth method [25]. Ag Kα X-ray data were collected on an Enraf-Nonius four-circle (CAD4) diffractometer at 293, 473, 673, 873 and 973 K for the two crystals, and also at 373 K for KRb12TP. For the high temperature data collection, we used our locally [26] improved gas-stream heating device [27], which ensures the crystal temperature remains constant within 3 K for 15 days. Table 1 gives some experimental details of the data collections.

The temperature was increased at a rate of 2 K per minute. Every 50 K, this rise was stopped to determine the lattice parameters. After the last data collection at 973 K, the lattice parameters have also been determined during temperature decrease every 50 K with the same procedure in order to check any possible hysteresis. At each temperature, successive centering procedures were performed until the sample had reached equilibrium ($\approx$ 2 hours). The change in the cell parameters and in the unit cell volume *versus* temperature are given in Figure 2, compared to those obtained for the pure RbTP [11] and KTP [24] crystals. No hysteresis appears. The evolution of solid solution cell parameters are similar to those obtained for RbTP and KTP. Especially for temperatures close to room temperature the perturbation in cell parameters induced by K exchange in RbTP is bigger than that obtained when substituting K by Rb in KTP: the quadratic form of the c parameter evolution for KTP, is also obtained for KRb12TP, whereas for KRb535TP this evolution is more linear as for RbTP.

In order to get accurate structure factors, multiple reflections, $(h, k, \pm l)$ and $(h, -k, \pm l)$, were collected. During the 15 days of each data collection, the maximum angular deviation periodically controlled (every 4 hours) was always less than the maximum allowed value (0.08°); owing to our improved sample holder [26], no reorientation occurred. The standard intensities remained extremely stable during the whole experiment.

Data reduction and error analysis were performed using the DREAR programs of Blessing [28]. After background subtraction, the intensities were corrected for Lorentz and polarization effects. A polynomial fit to the slight decay of the standard reflections intensities over the X-ray exposure time (3.3% for KRb535TP at T = 973 K; less than 1% for the other data), was applied to scale the data and to derive the instrumental instability coefficient (Tab. 1) used in the calculation of $\sigma^2(|F|^2) = \sigma_c^2(|F|^2) + (\langle p \rangle |F|^2)^2$ [29]. For KRb535TP, absorption ($\mu_{\text{calc.}} = 4.53$ mm^{-1}) and beam inhomogeneity corrections were calculated using the Gaussian integration method (ABSORB2 program) [30]. For KRb12TP, to reduce the effects of absorption, the sample was ground into a sphere (diameter 0.3 mm). In that case, absorption ($\mu_{\text{calc.}} = 2.30$ mm^{-1}) and beam inhomogeneity corrections were calculated by using SORTAV [31]: a spherical harmonic expansion in real form up to $l = 4$ for even order and $l = 3$ for odd order was found optimal to fit the absorption and beam inhomogeneity anisotropies. The differences between the transmission factors were not significant ($A_{\min} = 0.37(1)$ and $A_{\max} = 0.40(1)$).

3 Least squares refinements

For KRb535TP, room temperature x, y, z positions and U^{ij} anisotropic harmonic thermal displacement

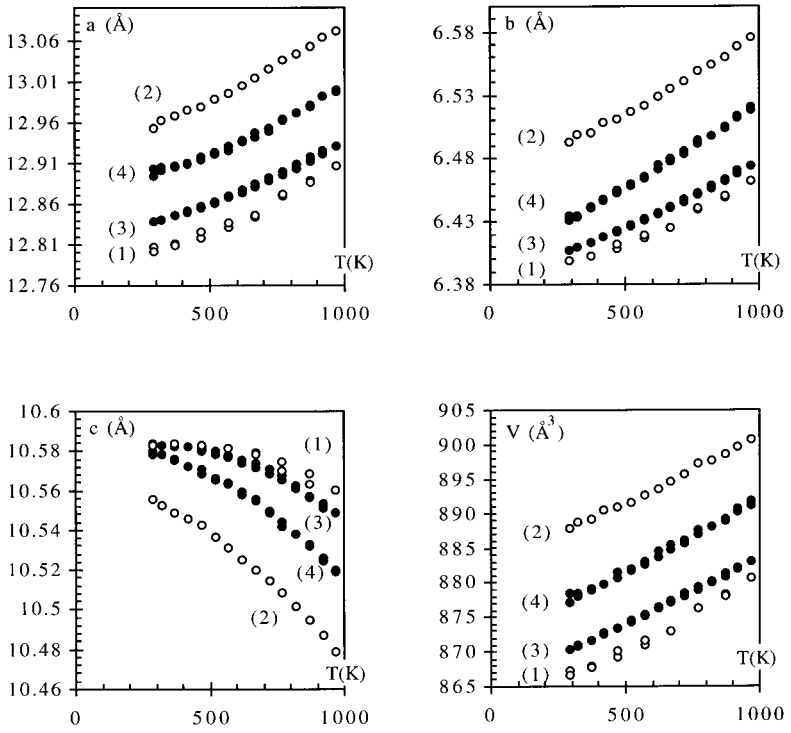

Fig. 2. Evolution of the cell volume (Å^3) and of the cell parameters a, b, c (Å) for (1) KTP [24], (2) RbTP [11], (3) KRb12TP and (4) KRb535TP *versus* temperature (K). Measurements obtained during the temperature increase and decrease are shown.

parameters of RbTP were used as starting parameters for the 293 K refinement using the Molly program [32]; for KRb12TP, those of KRb535TP were used. To refine the structure at the other temperatures, the parameters derived from the experiment at the preceding temperature were used as a starting point. In all cases, the K and Rb atoms were refined as ions (K^+ [33] and Rb^+ [34] scattering factors); the residual charge ($+2e^-$) was distributed over the ten oxygen atoms of the asymmetric unit. The core and radial valence scattering factors for non-Rb atoms were calculated from Clementi wavefunctions [33]. For each alkaline site (i = 1, 2) an average scattering factor was defined as:

$$\langle f^i_{\mathrm{Rb/K}} \rangle = (1-\alpha^i) f_{\mathrm{K}} + \alpha^i f_{\mathrm{Rb}} \qquad (1)$$

subjected to the constraint: $\alpha^1 + \alpha^2 = 2 \times 0.12 = 0.24$ for KRb12TP, $\alpha^1 + \alpha^2 = 2 \times 0.535 = 1.07$ for KRb535TP. The occupancies α^i were refined, together with the positional and thermal displacement parameters of the i sites. The anomalous dispersion of each atom [35] was taken in account. As in our previous work on RbTP [11] and KTP [24], three models were used to discuss the thermal displacement parameters of the alkaline ions.

3.1 Harmonic model (hm)

For both solid solutions, refinements of all x, y, z and U^{ij} parameters against the room temperature data (Tab. 1) led to excellent agreement indices R, Rw, Z. At higher temperatures, the anisotropic refinements did not converge well and gave non positive definite thermal parameters for some oxygen atoms; correlatively the residual density in the Rb/K regions increased a lot with temperature.

3.2 Anharmonic model (am)

Therefore, for K and Rb ions, the harmonic $T_0(\mathbf{H})$ Debye-Waller factors were corrected by the Gram-Charlier series expansion which is a Taylor-series-like expansion using the rectilinear Gaussian probability density functions and its successive derivatives [36]. As programmed in Molly [32], the thermal anharmonic $T(\mathbf{H})$ becomes:

$$T(\mathbf{H}) = T_0(\mathbf{H})[1 + \frac{i^3}{3!} C^{jkl} h_j h_k h_l + \frac{i^4}{4!} D^{jklm} h_j h_k h_l h_m + ...]$$

(where C^{jkl} and D^{jklm} are the third and the fourth order Gram-Charlier coefficients respectively.)

To reduce the number of parameters to a minimum and to compare more easily the change of the structure at each temperature [24], K/Rb atoms were anharmonically refined only up to the 4th order Gram-Charlier coefficients for every temperature. In spite of high correlation coefficients (> 0.80) between the 2nd order ($T_0(\mathbf{H})$) and the 4th or the 3rd orders, amplitudes of some anharmonic coefficients are very significant and their values increase with temperature. As in our previous work [11,24], the most

Table 1. Details of data collection and refinements.

$K_{0.88}Rb_{0.12}TiOPO_4$	Temperature (K)		293	373	473	673	873	973	293
	Lattice parameters (Å)	a	12.837(1)	12.844(1)	12.854(1)	12.881(1)	12.911(1)	12.930(1)	12.837(1)
		b	6.4059(4)	6.4122(5)	6.4212(5)	6.4397(6)	6.4612(7)	6.4733(6)	6.4066(5)
		c	10.582(1)	10.582(1)	10.580(1)	10.573(1)	10.557(2)	10.548(2)	10.582(1)
	$(\sin(\theta)/\lambda)_{max}$		1.16	1.16	1.16	1.16	1.16	1.16	1.16
	No of measured / unique (I>3σ) reflections		9075 / 3383	8537 / 3366	8598 / 3374	8946 / 3372	8520 / 3307	8149 / 3245	9450 / 3381
	Instrumental instability coefficient <p> (%)[28]		2.97	3.43	3.00	2.26	2.83	2.96	2.96
	R_{int} [(a)] (%)		1.71	1.85	2.07	2.17	2.07	2.00	2.00
	Model *hm*	Number of parameters	146						
	Scale factor		0.5716(8)	0.5673(7)	0.5641(8)	0.5558(9)	0.5415(12)	0.5380(15)	0.5654(7)
	R [(b)] (Rw [(c)]) (%)		2.04 (3.01)	2.03 (2.96)	2.17 (3.14)	2.62 (3.78)	3.45 (5.20)	4.19 (6.38)	2.18 (3.02)
	Goodness of fit Z [(d)]		1.33	1.2	1.33	1.67	2.01	2.42	1.33
	Model *am*	Number of parameters	196						
	Scale factor		0.5670(8)	0.5640(7)	0.5614(7)	0.5582(7)	0.5522(7)	0.5505(7)	0.5621(8)
	R [(b)] (Rw [(c)]) (%)		1.86 (2.77)	1.79 (2.59)	1.72 (2.52)	1.75 (2.48)	1.89 (2.70)	2.12 (2.78)	2.04 (2.82)
	Goodness of fit Z [(d)]		1.23	1.06	1.07	1.11	1.05	1.06	1.25
	Extinction parameters [(e)]		1.33(4)	1.23(3)	1.03(3)	1.35(4)	1.35(4)	0.85(3)	1.30(4)
	Model *sk*	Number of parameters	168						
	Scale factor				0.5648(6)	0.5608(7)	0.5554(7)	0.5530(7)	
	R [(b)] (Rw [(c)]) (%)				1.79 (2.61)	1.86 (2.62)	2.00 (2.85)	2.21 (2.91)	
	Goodness of fit Z [(d)]				1.11	1.16	1.10	1.10	
	Extinction parameters [(e)]				1.09(3)	1.40(4)	1.39(4)	0.88(3)	
$K_{0.465}Rb_{0.535}TiOPO_4$	Lattice parameters (Å)	a	12.902(1)		12.918(1)	12.946(1)	12.980(2)	12.999(2)	12.893(1)
		b	6.4339(8)		6.4547(7)	6.4793(8)	6.503(1)	6.520(1)	6.4305(7)
		c	10.580(1)		10.570(1)	10.555(2)	10.533(2)	10.519(2)	10.578(1)
	$(\sin(\theta)/\lambda)_{max}$		1.36		1.32	1.25	1.13	1.09	1.34
	No of measured / unique (I>3σ) reflections		14610 / 6024		11162 / 4733	9974 / 3811	9810 / 3175	4594 / 2749	13088 / 4854
	Instrumental instability coefficient <p> (%)[28]		1.92		2.23	2.14	1.27	1.26	2.24
	R_{int} [(a)] (%)		2.14		2.42	2.62	2.25	2.05	2.35
	Model *hm*	Number of parameters	146						
	Scale factor		0.2133(2)		0.2084(2)	0.2034(3)	0.1983(3)	0.2019(3)	0.2067(2)
	R [(b)] (Rw [(c)]) (%)		2.56 (2.88)		2.94 (3.19)	3.78 (4.28)	5.41 (6.46)	6.17 (7.63)	2.47 (2.88)
	Goodness of fit Z [(d)]		1.35		1.36	1.79	3.05	3.48	1.23
	Model *am*	Number of parameters	196						
	Scale factor		0.2141(2)		0.2098(2)	0.2079(2)	0.2064(3)	0.2062(3)	0.2091(2)
	R [(b)] (Rw [(c)]) (%)		2.41 (2.68)		2.40 (2.50)	2.44 (2.47)	2.61 (2.53)	3.23 (3.23)	2.27 (2.63)
	Goodness of fit Z [(d)]		1.27		1.07	1.04	1.20	1.45	1.13
	Extinction parameters [(e)]		0.15(1)		0.27(2)	0.25(2)	0.22(2)	0.14(2)	0.15(1)
	Model *sk*	Number of parameters	168						
	Scale factor				0.2093(2)	0.2080(2)	0.2071(3)	0.2064(3)	
	R [(b)] (Rw [(c)]) (%)				2.45 (2.56)	2.50 (2.54)	2.68 (2.60)	3.33 (3.35)	
	Goodness of fit Z [(d)]				1.09	1.06	1.23	1.53	
	Extinction parameters [(e)]				0.26(2)	0.26(2)	0.23(2)	0.14(2)	

[(a)] $R_{int}=(\Sigma|Y-Y_{mean}|)/\Sigma|Y|$, average of equivalent reflections in mm2 symmetry (sortav [31])
[(b)] $R=(\Sigma(|F_o|-|F_c|))/\Sigma|F_o|$, [(c)] $Rw=(\Sigma w(|F_o|-|F_c|)^2/\Sigma w|F_o|^2)^{1/2}$, [(d)] $Z=(\Sigma w(|F_o|-|F_c|)^2/(N-n))^{1/2}$, where F_o and F_c are the observed and calculated factors respectively, w is the weight assigned to each reflection, N is the number of independent reflections and n is the number of refined parameters.
[(e)] Isotropic extinction, type 1 with Lorentzian distribution.

important terms are C^{333} and D^{3333}. The anharmonic coefficients are more important in magnitude in the c direction and for site 1 than for site 2. This model improved the fit significantly (Tab. 1): however if the residual electron density peak heights around K/Rb sites calculated with the anharmonic refinements are smaller than those obtained with hm model, some physically meaningful peaks still exist especially at 973 K.

Within this am hypothesis, the average value of the thermal displacement parameter U_{eq} for each Ti, P and O atom ($U_{eq} = (U^{11}+U^{22}+U^{33})/3$) is linear *versus* temperature, and the straight line passes through the origin. The slopes (10^{-5} Å^{2}K^{-1} units) are 3.1 and 2.9 for O, 1.9 and 1.7 for Ti, 1.7 and 1.6 for P respectively for KRb535TP and KRb12TP. This is not the case for the cation sites thermal parameters, where the evolution *versus* temperature is similar (Fig. 3): despite a refinement at the 4th order of the Gram-Charlier coefficients for K^+/Rb^+, modelling each K^+/Rb^+ ion by a single site is not adequate. As for RbTP and KTP, it needs a more sophisticated model which splits the K^+/Rb^+ ions on several sites along the c axis. The distance between these pseudo atomic sites must decrease to zero at 0 K.

3.3 Splitting K/Rb sites (sk)

In this model each K^+/Rb^+ ion site has been split in two independent parts; the sum of the multiplicity of the two sets of pseudoatoms was constrained to be 1 during all refinements. At room temperature and at 373 K, we have observed very short distances between the two K^+/Rb^+ positions for each K/Rb(1) and K/Rb(2) site, leading to a too strong correlation between their x, y, z, U^{ij} and occupancy parameters. Therefore, at those temperatures, in order to compare the results with higher temperatures, the harmonic model (hm) will be used. At 473 K, x, y, z and U^{ij} calculated from the am refinement, were used as starting parameters. For each K^+/Rb^+ ion, two pseudoatoms labelled with subscripts ip (initial position) and sp (split position), were originally located at the $x_{K/Rb}$, $y_{K/Rb}$, $z_{K/Rb}$ am sites with their respective occupancies multiplied by 0.5. During the refinement process these two atoms split "naturally", with different occupancies, towards different positions (K/Rb(1, ip), K/Rb(1, sp) for site 1, K/Rb(2, ip) and K/Rb(2, sp) for site 2), corresponding respectively to the initial room temperature position, ip, and to the high temperature split position, sp. Due to high correlations (> 0.80) between the K/Rb pseudoatom parameters (occupancies, thermal displacement and z

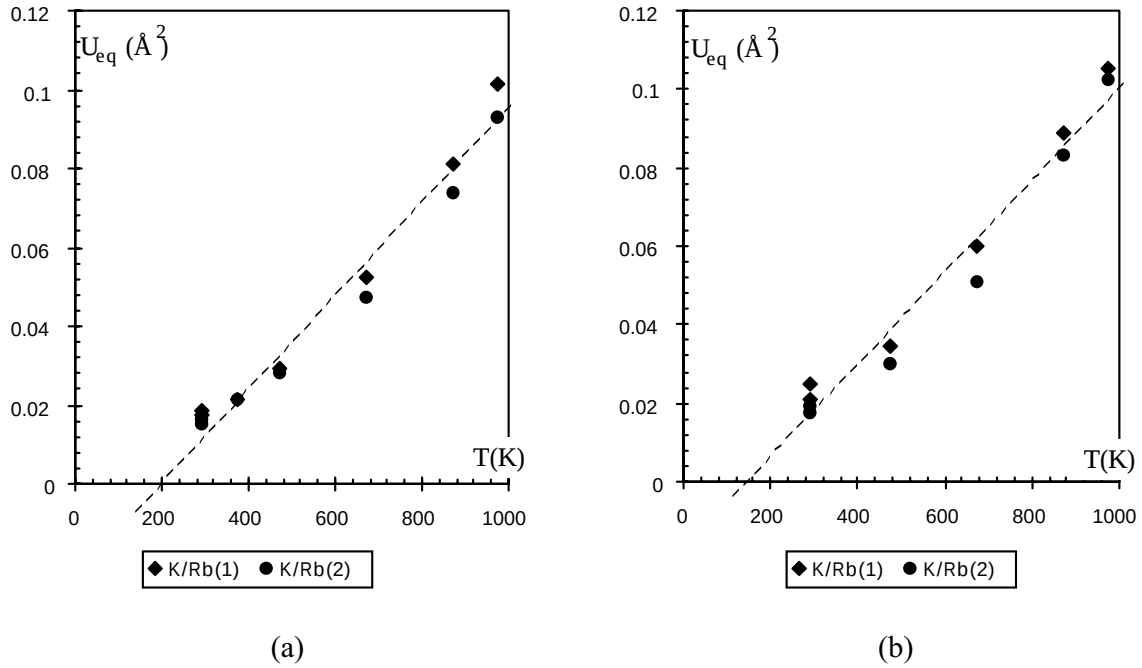

Fig. 3. Evolution of the average U_{eq} thermal motion value ($U_{eq} = (U^{11} + U^{22} + U^{33})/3$) (am model) for each alkaline site (Å^2) for (a) KRb12TP and (b) KRb535TP, *versus* temperature (K).

position), U^{ij} parameters of pseudo sites ip and sp were not refined together but alternately with all other parameters. For all higher temperatures, the same refinement procedure was applied and it improved the fit significantly (Tab. 1). For both solid solutions, Figure 4 gives the evolution *versus* temperature of the z coordinate of each pseudo atom site: at room temperature site 2 ($x = 0.10$, $y = 0.68$ and z_2) is mainly occupied by Rb ions; then increasing temperature reduces the difference between partial occupancies of both sites 1 and 2 leading at 973 K to an almost equipartition of the ions. One also observes that, as soon as each site is split, the sp site is mostly populated by Rb cations ($T = 473$, 673 K). Also, the Rb occupancy of the sp sites increases with temperature. More specifically for KRb535TP at 973 K both Rb(ip) and Rb(sp) occupancies are (0.25, 0.24) and (0.28, 0.30) for site 1 and site 2 respectively. In the case of KRb12TP at 973 K, these occupancies are (0.05, 0.06) and (0.04, 0.10) with an average e.s.d. of 0.02. Finally the inter site (ip-sp) distances do not appear to depend much on the substitution (0.769(3) and 0.68(1) Å, 0.67(1) and 0.65(1) Å, 0.722(2) and 0.649(7) Å, 0.728(3) and 0.622(8) Å, for RbTP, KTP, KRb12TP and KRb535TP respectively at 973 K).

However, our model is not totally satisfactory: if the evolution *versus* temperature of the average thermal displacement parameters U_{eq} of the K/Rb ions of ip sites is linear with an extrapolated value at 0 K close to the origin, this is not true for sp sites which do not exhibit such a linear relationship *versus* temperature (Fig. 5).

Then, to try to improve this model for KRb535TP and KRb12TP at 973 K, the contraints on the x, y, z and U^{ij} parameters of each K/Rb(1, sp) and K/Rb(2, sp) split positions were not applied, giving rise to two new pairs of sites: K(1, sp), Rb(1, sp) and K(2, sp), Rb(2, sp). For the refinement process, the x, y, z, U^{ij} and occupancies parameters obtained with the sk model were used as starting parameters. First, the alkaline positional parameters were refined alone. The two K/Rb(1, sp) and K/Rb(2, sp) sites split into K(1, sp), Rb(1, sp), K(2, sp) and Rb(2, sp) independent sites. Then, the major stages of refinements were: alkaline thermal parameters, all x, y and z parameters, all x, y, z and U^{ij} parameters, alkalines occupancies and finally all parameters. As previously, the U^{ij} parameters of the three pseudo-atoms pairs (K/Rb(1, ip), K/Rb(2, ip), K(1, sp), K(2, sp) and Rb(1, sp), Rb(2, sp)) were refined alternately due to high correlation (> 0.85) between these pseudoatom parameters. This sk model development improved the fit to the structure factors significantly: with fewer parameters than for the am refinement (186 parameters instead of 196), the residual factors ($R = 3.18\%$ and $R = 2.05\%$ at 973 K for KRb535TP and KRb12TP respectively) are lower than those found for the anharmonic model ($R = 3.33\%$ and $R = 2.21\%$ respectively). Positional and thermal parameters of these pseudo-atoms are given in Table 2. Positional, thermal and occupancy parameters obtained, at each temperature, with the am and the sk models are given in supplementary material and are available in the electronic version.

4 Discussion

4.1 Comparison with the pure KTP isostructure materials

As expected from our previous RbTP [11] and KTP [24] measurements, in the studied temperature range,

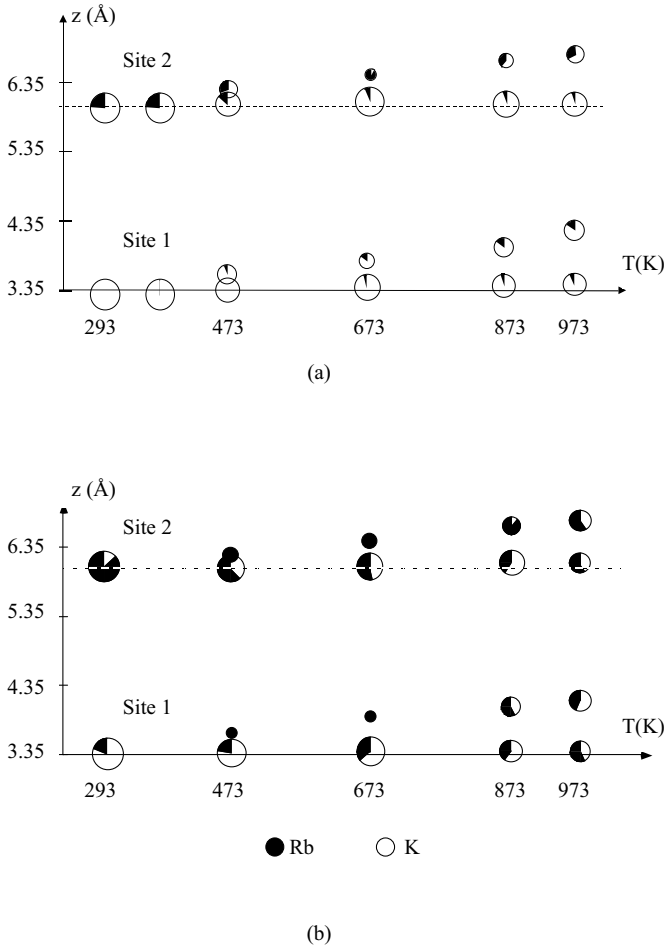

Fig. 4. Evolution of the potassium sites (see (i) in Fig. 1.) obtained with the two atoms split model (sk) for (a) KRb12TP and (b) KRb535TP, *versus* temperature (K). The distances are represented along the c axis and the dark and white surfaces of disks are proportional to the occupancy of Rb and K respectively in each pseudo-site.

the major effect on KRB12TP and on KRB535TP is the displacement of the K/Rb ions along the c axis. The split atom model shows that the initial room temperature position, ip of each K/Rb ion does not change and that its occupancy decreases in favor of the sp sites which move in the $+c$ direction to attain a global high temperature centrosymmetric structure (Fig. 4). Then the sp sites converge to the centrosymmetric images (the inversion center lies at (1/4, 1/4, 1/4) in the Pnan phase) of the ip positions which correspond to the hole sites proposed by Thomas and Glazer in their discussion about the possible ionic path [37] to explain KTP ionic diffusion properties. As in our study of RbTP and KTP, this work confirms the proposed ionic paths. In the same way, it has been observed that Rb ion exchange in KTP is more efficient (deeper and more rapid) on $-c$ face than on $+c$ face [38]. The ion exchange process is enhanced by the presence of a large number of vacancies in the crystal. By the ionic path proposed, the K/Rb^+ ions move more readily towards the $-Z$ surface, then the exchange process is expected to be more efficient at this end of the crystal. The physical reason for this difference between $+Z$ and $-Z$ given by Thomas and Glazer [37] is also confirmed by our results.

The necessity of the split atom model (with two pseudo sites for each alkaline site) in the KTP isostructure has also been shown for the germanate family [21]. The transition temperatures to the centrosymmetric phase (Pnan space group) of some of those compounds are much lower than for KTP and RbTP ($T_c = 272$ K for $TlSbOGeO_4$). The high temperature structure can then be accurately determined. Several groups [21,22] showed that in this centrosymmetric phase, alkaline atoms occupy two independent sites at a distance of less than 1 Å along the c axis. When the temperature reduces, those two sites give four positions and the structure is described in space group $Pna2_1$. Moreover, the distance between the split positions in the high temperature phase increases with the phase transition temperature. Then, as the phase transition temperature of RbTP is lower than that of KTP, Rb must reach more rapidly the centrosymmetric position. In accordance with this, the present study shows that Rb^+ ions are the first to occupy the sp positions (Fig. 4).

Contrary to our previous study of RbTP, the split site model for KRb535TP and KRb12TP is not optimal: the U^{ij} thermal motion evolution is not linear *versus* temperature for sp sites. Then, due to the differences between K and Rb mass and ionic radii [24] (about 6% [39]), the evolution of the alkaline ions in the solid solution is not similar to that of RbTP. The improvement of the split atom model with three pairs of pseudo atoms shows that the U_{eq} parameters of the Rb(sp) pair in KRb12TP are in the same order than the K/Rb(ip) values; and then, they seem to be linear *versus* temperature as they are in RbTP [11]. This is not the case for the K(sp) pair, as in KTP [24]. The Rb and K ions in KRb12TP have a similar behaviour as that found in RbTP and KTP respectively. This observation does not hold for KRb535TP (Tab. 2). Both the Rb and K behaviours are correlated (the two K(sp) and Rb(sp) sites need to be refined with different occupancies of K and Rb in each site, giving K/Rb(sp′) and K/Rb(sp) sites). Then in that case, the alkaline behaviour is not similar to that observed for RbTP or KTP but midway between them. This is confirmed by the evolution of the c parameters *versus* temperature. As already discussed in our previous high temperature study of KTP [24], the non linear c evolution for KRb12TP is correlated with the high thermal motion of the K(sp) sites. For KRb535TP, although the c value at room temperature is close to those of KTP and KRb12TP, the evolution *versus* temperature is more similar to that of RbTP.

Even if the split atom model may need to be developed, and contrary to the work on $TlTiOPO_4$ [40] which splits the sites by eight, an accurate study dealing with a model with a higher number of split atoms is not possible in our case. Due to the mass and radius differences of the K and Rb cations and to the order-disorder phenomenon, the correlation between thermal, occupancy and z position parameters is too high. Then, a discussion on the thermal

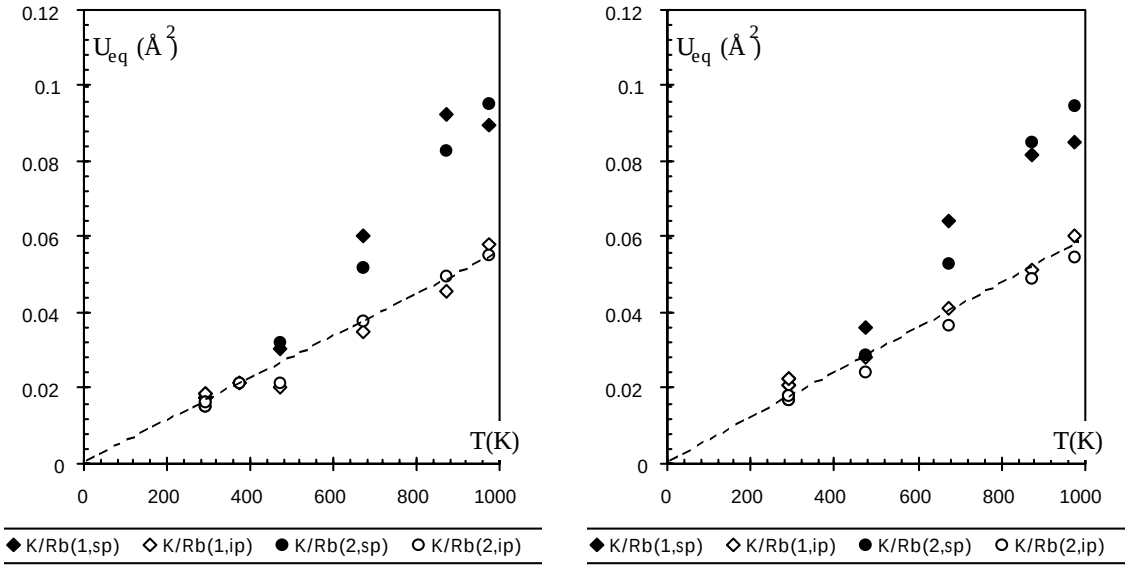

Fig. 5. Evolution of the average U_{eq} thermal motion value ($U_{eq} = (U^{11} + U^{22} + U^{33})/3$) (sk model) for each pseudo site (Å^2) for (a) KRb12TP and (b) KRb535TP, *versus* temperature (K).

Table 2. Positional, U_{eq} equivalent thermal (Å^2) and occupancy parameters obtained at 973 K with the splitting of K sites (sk) in the case of three pseudo-atoms in each site for KRb12TP and for KRb535TP.

	Fractional coordinates (*10^4)			Ueq (10^{4}Å^2)	Occupancy (10^3)
	x	y	z		
KRb12TP					
K(1,sp)	3898(3)	7892(5)	3636(13)	820(28)	521(12)
Rb(1,sp)	3893(4)	7900(10)	4296(8)	466(33)	59(1)
K(1,ip)	3834(1)	7861(3)	3166(4)	564(13)	373
Rb(1,ip)	3834	7861	3166	564	45(2)
K(2,sp)	1066(3)	7022(6)	1160(13)	702(28)	371(11)
Rb(2,sp)	1202(4)	7272(7)	1714(11)	551(41)	66
K(2,ip)	1027(1)	6925(4)	742(3)	552(9)	493
Rb(2,ip)	1027	6925	742	552	68(2)
KRb535TP					
K(1,sp)	3873(4)	7770(11)	3676(22)	621(60)	353(31)
Rb(1,sp)	3967(4)	8032(10)	4175(7)	686(32)	210(7)
K(1,ip)	3868(3)	7904(6)	3301(4)	680(20)	154
Rb(1,ip)	3868	7904	3301	680	281(8)
K(2,sp)	1198(9)	7212(16)	1913(10)	403(54)	127(9)
Rb(2,sp)	1069(2)	7031(5)	1242(10)	771(37)	380
K(2,ip)	1052(1)	6949(5)	753(3)	539(16)	294
Rb(2,ip)	1052	6949	753	539	197(6)

motion and the occupancies will not be reasonable. Recently, using one particle potentials (opp) calculations [41] on $Ag_2MnP_2S_6$ [42], Van der Lee *et al.* concluded on the nature of disorder: as temperature increases, Ag tends to move to higher co-ordination sites, giving a resolved disorder characterised by a double well potential. In the same way, a diffuse X-ray scattering study on $TlSbOGeO_4$ [23] shows that the description of disorder distributes Tl atoms over a considerable range of positions and not only over the two alkaline positions derived in the average structure determination [21]. Therefore, similar further studies of the behaviour of the KTP family *versus* temperature may give more information on the evolution of the ip and sp sites.

4.2 Order-disorder parameter

In the past decade, several studies at room temperature on solid solutions of the KTP family show preferential occupancy of the two alkaline cations onto one of the two independent sites. Table 3 gives a summary of these

Table 3. Occupancies of each alkaline cation in each site obtained for $M_{1-x}N_xAOBO_4$ at room temperature. The ionic radius ratio (R(N)/R(M)) [39] and the order-disorder S factor (Eq. (2)) are given for each case.

	site 1		site 2		R(N)/R(M)	S
$M_{1-x}N_xAOBO_4$	N	M	N	M		
$K_{0.59}Tl_{0.41}TiOPO_4$ [48]	0.2	0.8	0.62	0.38	1.05	0.51
$K_{0.82}Tl_{0.18}TiOPO_4$ [16]	0.062	0.938	0.314	0.686	1.05	0.67
$Rb_{0.77}Tl_{0.23}TiOPO_4$ [16]	0.23	0.77	0.238	0.762	0.99	0.02
$Na_{0.58}K_{0.42}TiOPO_4$ [12]	0.067	0.933	0.773	0.227	1.25	0.84
$Rb_{0.93}Cs_{0.07}TiOAs0_4$ [14]	0.026	0.974	0.11	0.89	1.07	0.62
$Rb_{0.69}Cs_{0.31}TiOAs0_4$ [14]	0.15	0.85	0.47	0.53	1.07	0.52
$Rb_{0.42}Cs_{0.58}TiOAs0_4$ [14]	0.405	0.595	0.74	0.26	1.07	0.39
$Rb_{0.29}Cs_{0.71}TiOAs0_4$ [14]	0.589	0.411	0.84	0.16	1.07	0.44
$Rb_{0.14}Cs_{0.86}TiOAs0_4$ [14]	0.789	0.211	0.943	0.057	1.07	0.57
$K_{0.5}Rb_{0.5}SnOPO_4$ [17]	0.36	0.64	0.64	0.36	1.06	0.28
$K_{0.5}Rb_{0.5}Sn_{0.5}Ti_{0.5}OPO_4$ [17]	0.23	0.77	0.77	0.23	1.06	0.54
$K_{0.86}Rb_{0.14}TiOPO_4$ [20]	0	1	0.286	0.714	1.06	1.00
$K_{0.84}Rb_{0.16}TiOPO_4$ [20]	0.038	0.962	0.282	0.718	1.06	0.76
$K_{0.535}Rb_{0.465}TiOPO_4$ [19]	0.128	0.872	0.801	0.199	1.06	0.72
$K_{0.57}Rb_{0.43}TiOPO_4$ [18]	0.12	0.88	0.73	0.27	1.06	0.72
$K_{0.465}Rb_{0.535}TiOPO_4$	0.207	0.793	0.863	0.137	1.06	0.70
$K_{0.88}Rb_{0.12}TiOPO_4$	0	1	0.24	0.76	1.06	1.00

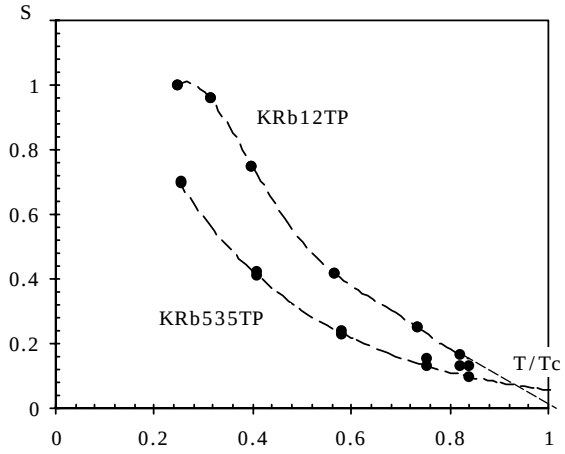

Fig. 6. Evolution of the S order-disorder factor (Eq. (2)) of both solid solutions, *versus* temperature (T/T_c). Dashed lines are guides to the eye.

results. To discuss the partitioning of the two cations in each site for any solid solution, we define the following order-disorder factor S:

$$S = \frac{\mathrm{To(Rb(2))} - \mathrm{To(Rb(1))}}{1 - |\mathrm{To(Rb(2))} + \mathrm{To(Rb(1))} - 1|} \qquad (2)$$

where To(Rb(i)) is the occupancy of Rb ions in site i ($i = 1$ or 2) for a solid solution like $K_{1-x}Rb_xTiOPO_4$. The value of this factor, which is equal to 0 for total disorder and 1 or -1 (depending of the reference site) for total order, is independent of the substitution percentage (x) in the solid solution.

When Sn replaces Ti in KTP [10], the deviation from the centrosymmetric Pnan structure of the SnO_6/PO_4 framework is smaller. Then, the two K-O cages volumes become more equivalent. The order-disorder factor S decreases when the percentage of Sn increases for a given value of x ($x \approx 0.5$): $S = 0.72$ in $K_{0.535}Rb_{0.465}TiOPO_4$ [19], $S = 0.54$ in $K_{0.5}Rb_{0.5}Sn_{0.5}Ti_{0.5}OPO_4$ [17] and $S = 0.28$ in $K_{0.5}Rb_{0.5}SnOPO_4$ [17]. The correlation between the cation ionic radius ratio and the evolution of S confirms the importance of the volume difference of the two alkaline sites: the radius difference between Rb and Tl of about 1% lead an almost complete disorder ($S = 0.02$) for $Rb_{0.77}Tl_{0.23}TiOPO_4$ [16]. In the same way, for $Na_{0.58}K_{0.42}TiOPO_4$ [12] with a ionic radius ratio R_K/R_{Na} of 1.25, the factor S is higher ($S = 0.84$) compared to $S = 0.72$ for $K_{0.57}Rb_{0.43}TiOPO_4$ [18] ($R_{Rb}/R_K = 1.06$). However, for $Rb_{0.42}Cs_{0.58}TiOAsO_4$ [14] with a higher ionic radius ratio than for $K_{0.535}Rb_{0.465}TiOPO_4$ [19] or $K_{0.57}Rb_{0.43}TiOPO_4$ [18], the disorder is more important ($S = 0.39$, 0.72 and 0.72 respectively). But in that case, As substitutes P and we cannot determine if the volume energy only could explain the phenomenon. Furthermore, in this discussion, the relative temperature T/T_c was not taken in account, as it will be later.

Figure 6 gives the evolution of the order-disorder factor S *versus* relative temperature for KRb12TP and KRb535TP. The phase transition temperature was obtained by interpolation of the temperature at which the SHG disappears against the $K_{1-x}Rb_xTP$ family [43] (T_c(KRb12TP) = 1188 K and T_c(KRb535TP) = 1158 K). The two structure refinement models (the anharmonic and the split site model) led to the same evolution: hence these models give the same values of occupancies in each site within the estimated standard deviation. At room temperature, the S values for KRb12TP and KRb535TP (respectively $S = 1.00$ and $S = 0.70$) are close to those calculated for $K_{0.86}Rb_{0.14}TiOPO_4$ [20] ($S = 1.00$) and

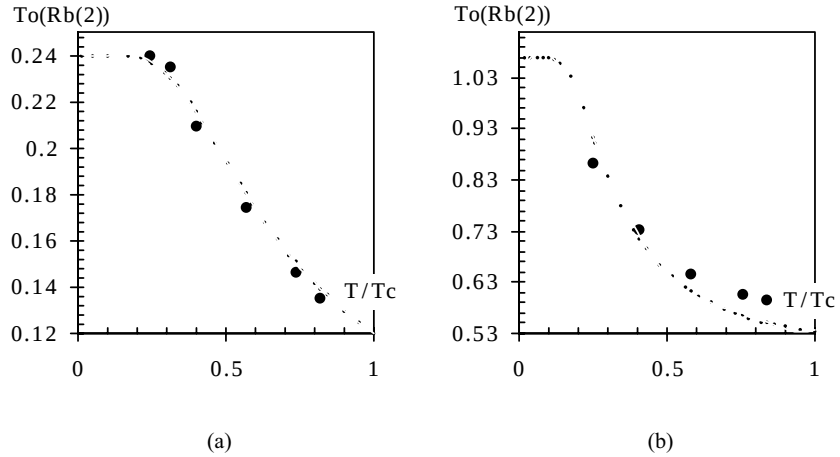

Fig. 7. Evolution of Rb occupancy (am model) in site 2 (To(Rb(2))) for (a) KRb12TP and (b) KRb535TP, *versus* temperature (T/T_c). The calculated values ("volume" potential-barrier model, Eq. (4)) are represented.

$K_{0.535}Rb_{0.465}TiOPO_4$ [19] ($S = 0.72$). As these crystals have been obtained differently, it appears that an order blocking temperature does not exist and that the order disorder phenomenon is governed by the ionic conductivity properties of the KTP family. This is confirmed by the evolution *versus* temperature: the high S values at room temperature decreases progressively to be close to zero near the phase transition temperature, T_c.

To understand accurately this phenomenon by a model, we will only consider the occupancy of Rb in site 2, To(Rb(2)) (Fig. 7). The other Rb and K occupancies may be obtained using the constraints on each site and on the substitution percentage (x) of Rb. To fit the evolution of To(Rb(2)), we use a simple potential-barrier model [44]. The two alkaline sites are considered as two wells of potential energy. The thermal motion of Rb ions allows jumping from one well to the other. The probability of jump Γ is proportional to $\exp(-U/kT)$ where U is the "depth" of the hole potential, T the temperature and k the Boltzmann constant. As the volume of the two sites is not equivalent, ε is the difference between the two potential energies. Then the probability of jump for Rb from site 1 to site 2 is To(Rb(1)) $\Gamma \exp(-\varepsilon/kT)$ and the probability of jump for Rb from site 2 to site 1 is To(Rb(2)) $\Gamma \exp(-\varepsilon/kT)$, hence in equilibrium:

$$\mathrm{To(Rb(1))}\Gamma \mathrm{e}^{\varepsilon/kT} = \mathrm{To(Rb(2))}\Gamma \mathrm{e}^{-\varepsilon/kT}. \qquad (3)$$

As $\mathrm{To(Rb(1))} = 2x - \mathrm{To(Rb(2))}$, we have:

$$\mathrm{To(Rb(2))} = 2x \frac{\mathrm{e}^{\varepsilon/kT}}{\mathrm{e}^{\varepsilon/kT} + \mathrm{e}^{-\varepsilon/kT}}\,. \qquad (4)$$

When the structure moves to the centrosymmetric space group Pnan [11,24], the difference between the two alkaline volumes may not be constant as ε. We have then calculated the evolution of the alkaline volumes *versus* temperature for both solid solutions (the calculation algorithm is given in the appendix). The volume evolution is proportional to the choice of the atomic radii. The results obtained with this method on KTP agree with the variation

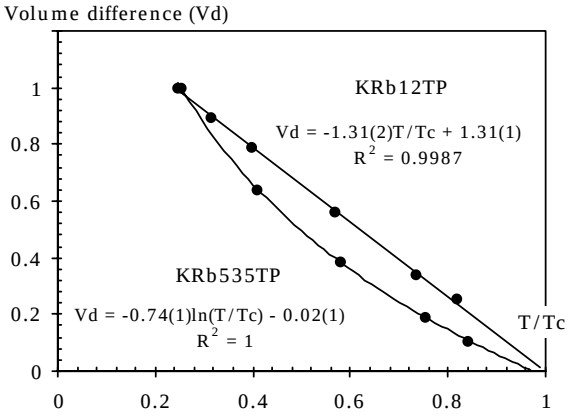

Fig. 8. Evolution of the volume difference between alkaline site 1 and 2 for both solid solutions, *versus* temperature (T/T_c). The fitting equations and their correlation coefficients are given.

of the atomic basins [45] determined by an electron density topology study [46] following Bader analysis [47]. Figure 8 gives the volume difference evolutions, normalised to 1 at room temperature, due to the high difficulty in obtaining an absolute volume. Then, the equations obtained (Fig. 8) through a linear (KRb12TP) or exponential (KRb535TP) fit were used to determine the evolution of ε *versus* temperature:

$$\begin{aligned} \varepsilon(T/T_c) &= u(1.31 - 1.31T/T_c) \quad \text{for} \quad \text{KRb12TP} \\ \varepsilon'(T/T_c) &= u'(-0.02 - 0.74\ln(T/T_c)) \quad \text{for} \quad \text{KRb535TP}. \end{aligned} \qquad (5)$$

As the volume differences have been normalised and to take in account the activation energy [44], ε was scaled to give a calculated To(Rb(2)) value equal to the experimental one at room temperature ($u = 0.18$ and $u' = 0.065$). Considering this very simple "volume" model, the calculated values (dotted line) are in excellent agreement with experiment for KRb12TP and agree well for KRb535TP in the low temperature region ($T/T_c < 0.5$) (Fig. 7).

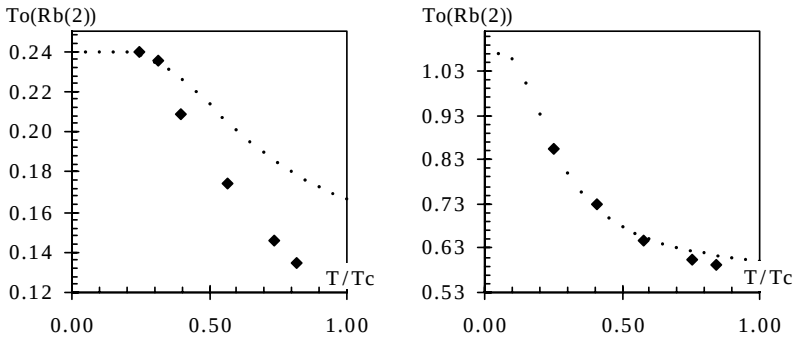

Fig. 9. Evolution of Rb occupancy in site 2 (To(Rb(2))) for (a) KRb12TP and (b) KRb535TP calculated with the "interaction" potential-barrier model, *versus* temperature (T/T_c).

Table 4. Order-disorder S value for solid solutions obtained at 293 K and calculated (S_c) with the "interaction" potential-barrier model for the same relative temperature ($T/T_c = 0.24$).

$M_{1-x}N_xAOBO_4$	Tc (K)	Tc (K) used	293/Tc	S	v	T/Tc	S_c
$K_{0.59}Tl_{0.41}TiOPO_4$ [44]	1082 [48]						
	1064 [49]	1073	0.27	0.51	0.249	0.24	0.59
$Na_{0.58}K_{0.42}TiOPO_4$ [12]	1226 [49]	1226	0.24	0.84	/	0.24	0.84
$Rb_{0.42}Cs_{0.58}TiOAs0_4$ [14]	1027 [14]						
	1001 [43]*	1014	0.29	0.39	0.111	0.24	0.48
$K_{0.57}Rb_{0.43}TiOPO_4$ [17]	1143 [43]*	1143	0.26	0.72	0.304	0.24	0.74

* Values obtained by the interpolation of the SHG vanishing temperatures against the solid solution family.

To improve the calculated values in the high temperature region, we replaced the volume evolution term by an "interaction" term between alkaline sites. The probability of jump for Rb in site 2 is different when site 1 is partially occupied by Rb ions. Then, the difference between the two potential, ε, should be proportional to To(Rb(2)) ($\varepsilon(T/T_c) = v$ To(Rb(2)), where v is obtained empirically at room temperature: 2.450 and 0.204 for KRb12TP and KRb535TP respectively). In this interaction model, the fit of experimental values for KRb535TP is better than with the "volume" model. But it is not the case for KRb12TP (Fig. 9). Then, if in both cases there are interactions between alkaline ions and the framework, the constraints in KRb12TP are less important than those in KRb535TP. For few percent of Rb in KTP (*i.e.* KRb12TP), the alkaline sites may accommodate the bigger ions by means of the elasticity of the structure. For a higher Rb percentage (*i.e.* KRb535TP), the elasticity is not enough, and the interactions between the two alkaline sites govern the order-disorder evolution. This confirms the previous discussion about the behaviour of K and Rb in both solid solutions in comparison of KTP and RbTP.

As the "interaction" potential-barrier model does not need information about the volume evolution of the alkaline sites and as it gives correct values of half substituted solid solutions, the order-disorder S parameter has been extrapolated at the same relative temperature for some of the compounds given in Table 3. Table 4 gives the resulting corrected S values. For the calculations, T_c needs to be known for each compound. As T_c is difficult to obtain and as values given by alternative methods are different, depending also on the crystal quality, the error on the T_c estimate cannot be accurately determined. However, it does not change the previous discussion on the comparison of solid solutions given in Table 3.

The extrapolated value of S at 0 K gives a total order ($S = 1$) whatever the solid solution. But the ionic conductivity decreases with temperature. Then at low temperature, the competition between ionic conductivity and spontaneous polarisability is more important. Due to this spontaneous polarisability, the total order ($S = 1$) may not be reached at 0 K for some solid solutions. The barrier-potential models do not take this phenomenon into account.

5 Conclusion

Even if the split atom model describes more precisely the evolution of the alkaline sites *versus* temperature, the same order-disorder parameter for each alkaline solid solution is obtained whatever the structure refinement model (sk or am). Moreover, the simple thermodynamic barrier-potential model gives results which are in excellent agreement with experimental values. Above room temperature, those models show the importance of the volume energy

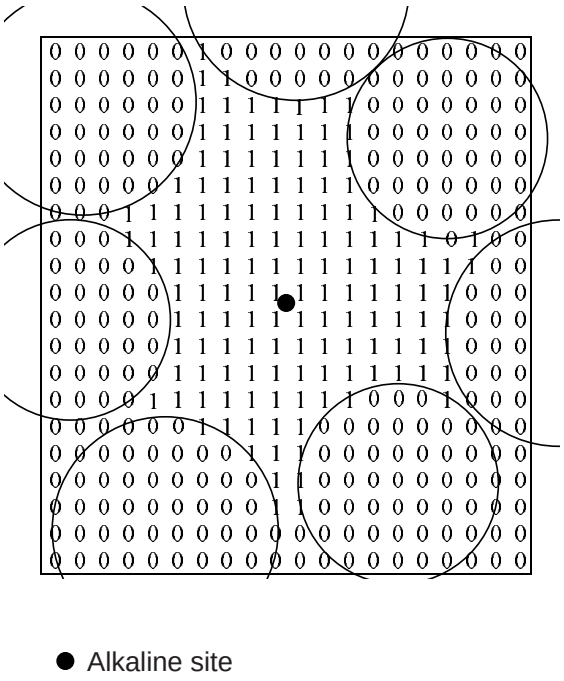

Fig. 10. Two-dimensional example of $t(x_n, y_n, z_n)$ assignment (Eq. (5)).

in the order-disorder phenomenon, and more generally in the ionic conductivity properties of these materials. The evolution of the alkaline volume is due to the constraints of alkaline ion on the framework. But a more complex model which describes precisely the evolution of these volume differences and calculates the exact activation potential is needed to show the interaction of those constraints on the polarisability of the Ti-O bond in the nonlinear properties.

P. Delarue is grateful to the Région Lorraine (France) for a doctoral fellowship. The support of University Henri Poincaré, Nancy I, University of Bourgogne and CNRS is also gratefully acknowledged.

Appendix: Calculation of the alkaline site volumes

As the oxygen cages of the alkaline sites are very distorted, the choice of neighbour atoms for the calculation of simple polygon volumes is difficult. Different tests (eight or nine oxygen neighbours for each alkaline site) have been realized leading to results without physical meaning. To compute the volume of these cages, therefore we have used another algorithm. The volume has been obtained by integration of the free space seen by a point placed on the alkaline sites which is defined by neighbour atoms in a box centred on this point. In this box limited by ($x_{\max}$, $x_{\min}$), ($y_{\max}$, $y_{\min}$) and ($z_{\max}$, $z_{\min}$), atoms are defined by a sphere using the centre coordinates x_i, y_i, z_i and the radius R_i as parameters. The cage site volume is given by:

$$V = \sum_{x_n=x_{\min}}^{x_{\max}} \sum_{y_n=y_{\min}}^{y_{\max}} \sum_{z_n=z_{\min}}^{z_{\max}} t\,(x_n, y_n, z_n)\,\delta x \delta y \delta z \quad \text{(A.1)}$$

with $x_{n+1} = x_n + \delta x, y_{n+1} = y_n + \delta y, z_{n+1} = z_n + \delta z$ and $t(x_n, y_n, z_n) = 0$ or 1: $t(x_n, y_n, z_n) = 0$ if the line going from (x_n, y_n, z_n) to the centre of the box is intercepted by one of the spheres. Figure 10 is a simple 2 dimensional example of the assignment of $t(x_n, y_n, z_n)$. For our calculation, parameters used are: a box of $6 \times 6 \times 6$ Å^3, $\delta x = \delta y = \delta z = 10^{-2}$ Å, $R_{\mathrm{P}} = 1.0$ Å, $R_{\mathrm{Ti}} = 1.0$ Å [39] and $R_{\mathrm{O}} = 1.76$ Å [50]. As the choice of the sphere radius is important, a test was undertaken with the oxygen radii reduced by 15% ($R_{\mathrm{O}} = 1.5$ Å). For example, with KRb535TP a change of 6% on the relative volume difference between alkaline site 1 and 2 is obtained, which represents less than a 1% change in the evolution between room temperature and 973 K; this is negligible in equation (5).

References

1. R. Masse, J.C. Grenier, Bull. Soc. Franc. Mineral. Cristall. **94**, 437 (1971).
2. I. Tordjman, R. Masse, J. C. Guitel, Z. Kristallogr. **139**, 103 (1974).
3. V.K. Yanovskii, V.I. Voronkova, Phys. Stat. Sol. (a) **93**, 665 (1986).
4. D.K.T. Chu, H. Hsiung, L.K. Cheng, J.D. Bierlein, IEEE Trans. Ultrason. Ferroelectr. Frequency Control **40**, 819 (1993).
5. W.T.A. Harrison, T.E. Gier, G.D. Stucky, A.J. Schultz, Mat. Res. Bull. **30**, 1341 (1995).
6. A. El Haidouri, J. Durand, L. Cot, Mat. Res. Bull. **25**, 1193 (1990).
7. M.L.F. Phillips, W.T.A. Harrison, T.E. Gier, G. D. Stucky, SPIE **1104**, 225 (1989).
8. M.L.F. Phillips, W.T.A. Harrison, G.D. Stucky, SPIE **1561**, 84 (1991).
9. G.D. Stucky, M.L.F. Phillips, T.E. Gier, Chem. Mater. **1**, 492 (1989).
10. P.A. Thomas, A.M. Glazer, B.E. Watts, Acta. Cryst. B **46**, 333 (1990).
11. P. Delarue, C. Lecomte, M. Jannin, G. Marnier, B. Menaert, Phys. Rev. B **58**, 5287 (1998).
12. S.J. Crennell, R.E. Morris, A.K. Cheetham, R.H. Jarman, Chem. Mater. **4**, 82 (1992).
13. J.D. Bierlein, A. Ferretti, L.H. Brixner, W.Y. Hsu, Appl. Phys. Lett. **50**, 1216 (1987).
14. a) M.N. Womersley, P.A. Thomas, D.L. Corker, Acta. Cryst. B **54**, 635 (1998); b) Z.W. Hu, P.A. Thomas, W.P. Risk, Phys. Rev. B **58**, 6074 (1998).
15. G. Marnier, united states patent CNRS 4961819 (1990).
16. M. Jannin, C. Kolinsky, G. Godefroy, B. Jannot, N.I. Sorokina, D.Y. Lee, V. I. Simonov, V.I. Vronkova, V.K. Yanoviskii, Eur. J. Solid State Inorg. Chem. **33**, 607 (1996).
17. S.J. Crennell, A.K. Cheetham, J.A. Kaduk, R.H. Jarman, J. Mater. Chem. **2**, 785 (1992).

18. W.T.A. Harrison, M.L.F. Phillips, G.D. Stucky, Z. Kristall. **210**, 295 (1995).
19. P.A. Thomas, S.C. Mayo, B.E. Watts, Acta. Cryst. B **48**, 401 (1992).
20. P.A. Thomas, R. Duhlev, S.J. Teat, Acta. Cryst. B **50**, 538 (1994).
21. E.L. Belokoneva, K.S. Knight, W.I.F. David, B.V. Mill, J. Phys. Cond. Matter. **9**, 3833 (1997).
22. J.F. Favard, A. Verbaere, Y. Piffard, M. Tournoux, Eur. J. Solid State Inorg. Chem. **31**, 995 (1994).
23. T.R. Welberry, S.C. Mayo, J. Appl. Cryst. **31**, 154 (1998).
24. P. Delarue, C. Lecomte, M. Jannin, G. Marnier, B. Menaert, J. Phys. Cond. Matter **11**, 4123 (1999).
25. G. Marnier, B. Boulanger, B. Menaert, M. Metzger, French patent CNRS No 8700811 (1987).
26. P. Delarue, M. Jannin, J. Appl. Cryst. **32**, 824 (1999).
27. R. Argoud, J.J. Capponi, J. Appl. Cryst. **17**, 420 (1984).
28. R.H. Blessing, Cryst. Rev. **1**, 3 (1987).
29. L.E. McCandlish, G.H. Stout, L.C. Andrews, Acta Cryst. A **31**, 245 (1975).
30. G.T. DeTitta, J. Appl. Cryst. **18**, 75 (1985).
31. R.H. Blessing, Acta Cryst. A **51**, 33 (1995).
32. (a) N.K. Hansen, P. Coppens, Acta Cryst. A **34**, 909 (1978); (b) N.K. Hansen, *MOLLY: Aspherical pseudo atom refinement on X-ray diffraction data*, LCM^{3}B, University Henry Poincaré, Nancy I, France.
33. E. Clementi, IBM J. Res. Dev. (Suppl.) **9**, 2 (1965).
34. D. Rez, P. Rez, I. Grant, Acta Cryst. A **50**, 481 (1994).
35. E.N. Maslen, A.G. Fox, M.A. O'Keefe, *International Tables for X-ray Crystallography C* (1992) p. 219.
36. J.A. Ibers, W.C. Halmilton, *International Tables for X-ray Cryst (1974)*, Vol. IV.
37. P.A. Thomas, A.M. Glazer, J. Appl. Cryst. **24**, 968 (1991).
38. C.J. Van Der Poel, J.D. Bierlein, J.B. Brown, S. Colak, Appl. Phys. Lett. **57**, 2074 (1990).
39. R.D. Shannon, Acta. Cryst. A **32**, 751 (1976).
40. M.K. Blomberg, M.J. Merisalo, N.I. Sorokina, D.Y. Lee, I.A. Verin, V.I. Voronkova, V.K. Yanovskii, V.I. Simonov, Crystallogr. Rep. **43**,748 (1998).
41. R. Bachmann, H. Schultz, Acta. Cryst. A **40**, 668 (1984).
42. A. Van der Lee, F. Boucher, M. Evain, R. Brec, Z. Kristall. **203**, 247 (1993).
43. B. Boulanger, Ph.D. Thesis, University Henri Poincarré, Nancy I (1989).
44. J. Philibert, *Atom movements diffusion and mass transport in solids* (Les Editions de Physique, 1991).
45. M. Souhassou, R.H. Blessing, J. Appl. Cryst. **32**, 210 (1999).
46. P. Delarue, C. Lecomte, M. Jannin, M. Souhassou (in preparation).
47. R.W.F. Bader, *Atoms in molecules. A quantum theory* (Plenum Press, Oxford, England University press, 1990).
48. V.I. Voronkova, V.K. Yanoviskii, D.Y. Lee, N.I. Sorokina, I.A. Verin, N.G. Furmanova, V.I. Simonov, Kristallografiya **39**, 430 (1994).
49. V.I. Voronkova, E.S. Shubentsova, V.K. Yanovskii, Izvestiya Akademii Nauk SSSR **26**, 143 (1990).
50. Handbook of Chemistry and Physics, Robert C. Weast, 62nd edition (1981-1982).